Rare Metal Materials and Engineering
Volume 47, Issue 7, July 2018
Online English edition of the Chinese language journal

Available online at www.sciencedirect.com
ScienceDirect

Cite this article as: Rare Metal Materials and Engineering, 2018, 47(7): 1965-1972.

ARTICLE

Corrosion Behavior of P110 Tubing Steel in the CO_2-saturated Simulated Oilfield Formation Water with Element Sulfur Addition

Miao Jian[1,2], Yuan Juntao[2], Han Yan[2], Xu Xiuqing[2], Li Lei[2], Wang Ke[2]

[1] Xi'an Jiaotong University, Xi'an 710049, China; [2] State Key Laboratory of Performance and Structural Safety for Petroleum Tubular Goods and Equipment Materials, Tubular Goods Research Institute of CNPC, Xi'an 710077, China

Abstract: With continuously growing oil and gas demand, exploitation of highly sour reservoirs brings large corrosion risks due to the coupling effects of corrosive factors including elemental sulfur, CO_2, and formation water. In the present work, corrosion behavior of P110 tubing steel in simulated oilfield formation water containing elemental sulfur and CO_2 was investigated by immersion tests and electrochemical measurements. The results indicate that increasing temperature accelerates the corrosion rate of P110 tubing steel, promotes the formation of iron sulfide, and causes serious pitting corrosion. However, influence of temperature varies in different temperature range mainly due to the different corrosion-controlling species like CO_2 at low temperatures and elemental sulfur at high temperatures. Based on the results, the coupling effects of elemental sulfur and carbon dioxide were discussed.

Key words: P110 tubing steel; elemental sulfur; corrosion; formation water; CO_2 corrosion

Global oil and gas demand has been growing continuously, so that exploitation and production condition of new oil and gas resources becomes more and more severe[1]. In recent years, highly sour reservoirs with harsh environment are being exploited, where deposit of elemental sulfur in the pipeline systems can cause serious corrosion[2]. Furthermore, the presence of CO_2 and H_2S in the sour gas makes the environments more corrosive and the corrosion mechanism of metallic tubing steels more complicated. In the harsh environment containing elemental sulfur, CO_2 and H_2S, most metallic materials for tubing, casting and pipelines even Ni-based alloys would suffer severe corrosion and increase the risk of corrosion failure[3,4].

During highly-sour oil and gas exploitation, elemental sulfur is usually transported from the gas reservoir to the ground gathering system in three ways[5]: chemical reaction with hydrogen sulfide, dissolution in polymer alkanes, and carrying by high speed airflow in terms of micro droplet. As the temperature and pressure changes, elemental sulfur particles precipitate from natural gas and deposit, which may cause following hazards[6]: gas fluid channel decrease, pipe blockage, corrosion perforation and cracking.

Corrosion of carbon steels in CO_2 environment has been characterized widely in the past decades [7-19]. It was indicated that plenty of factors including temperature, CO_2 pressure, flow rate, chloride concentration, chemical composition, microstructures and so on affected the corrosion rate and scale property. Regarding the effect of temperature, some incongruous results were reported, possibly due to the coupling effects among different influencing factors rather than single temperature change. The addition of elemental sulfur can significantly influence the corrosion of carbon steels by increasing corrosion rate and promoting pitting corrosion[20,21].

The presence of elemental sulfur would affect the corrosion mechanism and then the corrosion products. Although iron sulfide is often the corrosion product of elemental sulfur corrosion and hydrogen sulfide corrosion,

Received date: July 14, 2017
Foundation item: National Natural Science Foundation of China (51301202, 21506256)
Corresponding author: Yuan Juntao, Ph. D., State Key Laboratory of Performance and Structural Safety for Petroleum Tubular Goods and Equipment Materials, Tubular Goods Research Institute of CNPC, Xi'an 710077, P. R. China, Tel: 0086-29-81887591, E-mail: yuanjuntaolly@163.com

the corrosion mechanism is far different. For the hydrogen sulfide corrosion, the corrosion process is usually involved in dissolution and dissociation of hydrogen sulfide in water, and formation of iron sulfide. For the elemental sulfur corrosion, the process is more complicated due to the core corrosion possibly induced by solid particles or deposits. Even though the mechanism of elemental sulfur corrosion is still indefinite, acidification of sulfur in aqueous solution below the melting point of elemental sulfur is usually considered as the main corrosion cause[22]. However, the field experience seems more complicated due to the co-existence of elemental sulfur, H_2S and CO_2 in highly sourer gas field, so that the corrosion mechanism is still open to debate.

With these considerations, the present work was aimed to study influences of temperature on the corrosion of P110 tubing steel in the CO_2-saturated simulated oilfield formation water with element sulfur addition. Based on the results, the corrosion mechanism affected by coupling effects among several corrosive factors was discussed at last.

1 Material and Methods

1.1 Materials and test solutions

In the present study, P110 tubing steel was studied with chemical composition as listed in Table 1. It can be seen from Fig.1 that the microstructure of P110 tubing steel is homogeneous, comprising tempered sorbite, and has no obvious rolling texture features. Samples with dimensions of 40 mm×10 mm×4 mm for immersion corrosion tests and coupons with dimensions of 10 mm×10 mm×4 mm for electrochemical tests were prepared from P110 tubes. All samples were ground by abrasive silicon carbide paper to 1000# and cleaned in acetone for 5 min ultrasonically.

Simulated oilfield formation water was prepared with deionized water and analytical reagents according to the chemical composition as listed in Table 2. In particular, 5 g/L elemental sulfur was added.

1.2 Immersion corrosion test

All immersion corrosion tests were performed isothermally. Prior to tests, high purity N_2 was purged into the test container for 2 h to remove dissolved oxygen in test solutions, and then high purity CO_2 was introduced for 1 h to saturate the test solutions. After tests, some specimens were cleaned by appropriate chemical solution to keep the corrosion products down and then cleaned with deionized water and ethanol. The average corrosion rate V_{corr} was calculated by Eq.(1) based on the mass change of specimens.

$$V_{corr} = 8.76\times(m_0-m_1)/(St\rho) \quad (1)$$

where m_0 is the mass of samples before the test (g), m_1 is the mass of samples after the test (g), t is the corrosion duration (h), S is the surface area of specimen (m^2), and ρ is the density of specimen (g/cm^3). Other specimens were rinsed with distilled water, and used to characterize the corrosion products. In the present work, test temperatures were set as 30, 50, 70, and 90 °C and the test duration was set as 120 h.

1.3 Electrochemical tests

Polarization curves and electrochemical impedance spectroscopy (EIS) measurements were carried out in a CS370 electrochemical workstation. The conventional three-electrode system was used, where P110 specimen was the working electrode, a saturated calomel electrode (SCE) was the reference electrode, and a pair of graphite poles was the auxiliary electrode. All electrochemical tests were performed at a constant potential scan rate of 0.5 mV/s.

1.4 Characterization methods

The corroded samples were characterized by microstructure investigation, phase identification and chemical composition analysis. A Scanning Electron Microscopy (SEM) was employed to investigate the scale microstructures, an X-ray Diffraction (XRD) spectrometer with Cu Kα radiation was utilized to identify the corrosion products, and an Energy Dispersive Spectrum (EDS) detector was used to analyze the chemical compositions of corrosion scales.

Table 1 Chemical composition of P110 tubing steel (wt%)

C	Si	Mn	P	S	Cr	Ni	Ti	V	Fe
0.260	0.200	1.400	0.009	0.003	0.150	0.010	0.030	0.012	Bal.

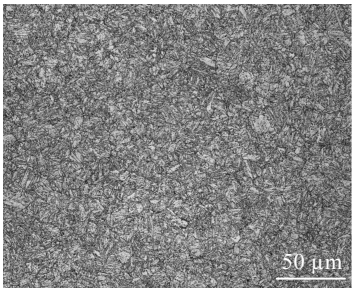

Fig.1 Microstructure of P110 tubing steel

2 Results

2.1 Characteristic of corrosion

Fig.2 depicts the corrosion rates of P110 tubing steel in the simulated environment at different temperatures for 120 h exposure. Overall, corrosion rates of P110 tubing steel increase with temperature increasing. Evidently, the V_{corr}-T relationship can be divided into three parts according to the slope as indicated in Fig.2. In the first region (30~50 °C), the extremely low slope suggests the slight temperature effect on the corrosion rate of P110 tubing steel. In the second region

Table 2 Chemical composition of simulated oilfield formation water

Chemical reagent	$MgSO_4·7H_2O$	$CaSO_4$	Na_2CO_3	$NaHCO_3$	Na_2SO_4	NaCl	S
Content/g·L^{-1}	0.18	0.642	0.557	5.31	8.732	16.48	5

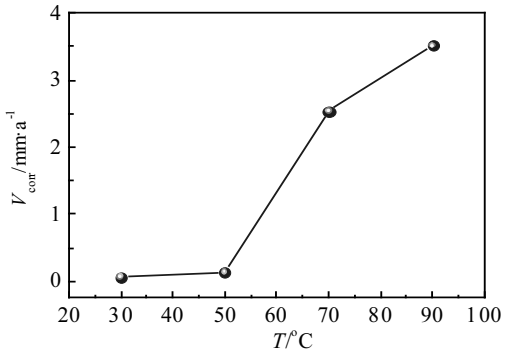

Fig.2 Corrosion rates of P110 tubing steel

(50~70 °C), the steep slope indicates the significant temperature dependence on the corrosion rate. In the third region (70~90 °C), the slope becomes low gradually, indicating that the influence of temperature is lowered possibly due to the rapid formation of thick corrosion products.

Concerning the CO_2 corrosion, it is often considered that temperature would affect corrosion rate of carbon steels strongly. At temperatures below 60 °C, protective $FeCO_3$ films cannot form unless the pH is high enough; therefore, corrosion rate would increase with temperature. Above 60 °C, the decrease of $FeCO_3$ solubility would result in the increase of protectiveness of $FeCO_3$ films with temperature, so that the corrosion rate would be reduced with temperature increasing[23,24]. The addition of elemental sulfur seems to make the corrosion more complex possibly due to the complicated influence of temperature on the CO_2 corrosion and elemental sulfur corrosion.

Fig.3 presents the surface morphologies of P110 tubing steel corroded in the simulated environment at different temperatures. At 30 °C, the corroded specimen shows a thin and smooth surface, and the corrosion film is thin considering the clear grinding marks (Fig.3b). At 50 °C, some white particles appear on the surface of the corroded specimen, and EDS analysis shows high concentration of S for such particles. In addition, localized spalling can be observed in Fig.3d. At 70 °C, serious corrosion and evident exfoliation can be seen in Fig. 3e. At 90 °C, much more serious corrosion, large particles and deep holes can be seen in Fig. 3h. With temperature increasing, more S can be detected on the surface films by EDS, indicating severe elemental sulfur corrosion at higher temperatures.

Fig.4 shows the XRD patterns for the surface films formed on P110 tubing steel. At 30 °C, the corrosion is slight so that the surface film is too thin to detect. At 50 °C, the surface film is composed of $FeCO_3$. At 70 °C and 90 °C, the surface films are composed of $FeCO_3$ and FeS. When temperature increases from 70 °C to 90 °C, the peaks for FeS become stronger. In all cases, peaks for P110 tubing steel are strong, suggesting the surface films on the specimens are thin.

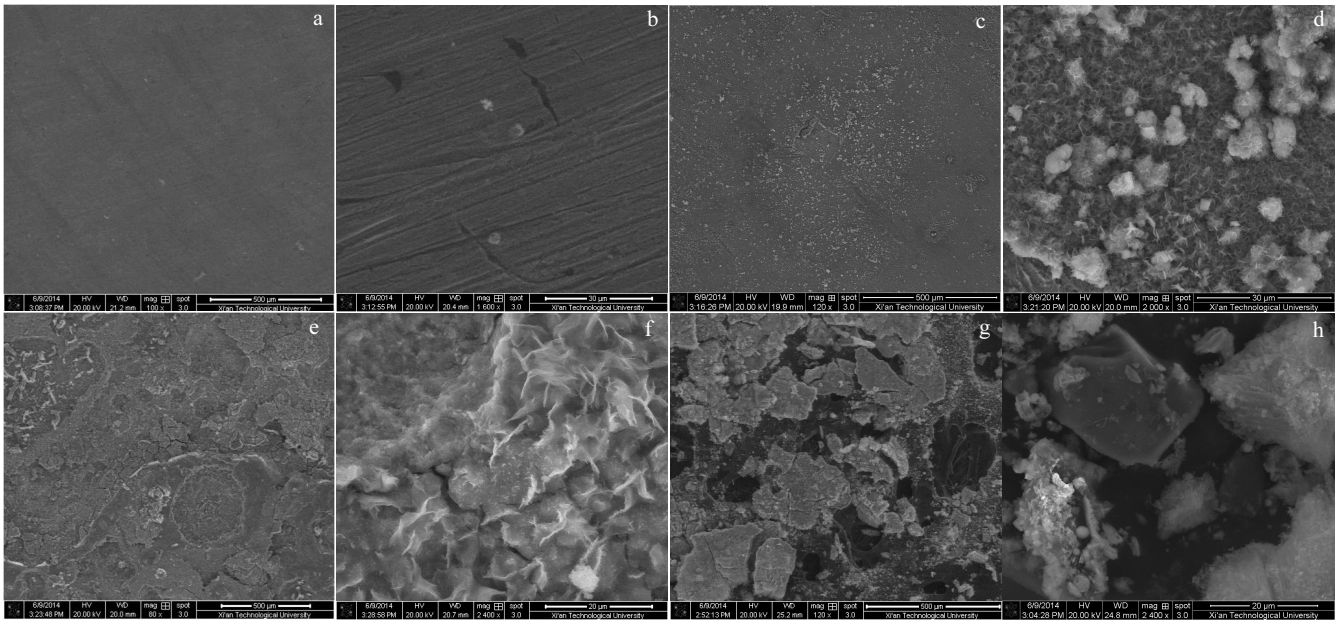

Fig.3 Surface morphologies of P110 tubing steel corroded at different temperatures: (a, b) 30 °C, (c, d) 50 °C, (e, f) 70 °C, and (g, h) 90 °C

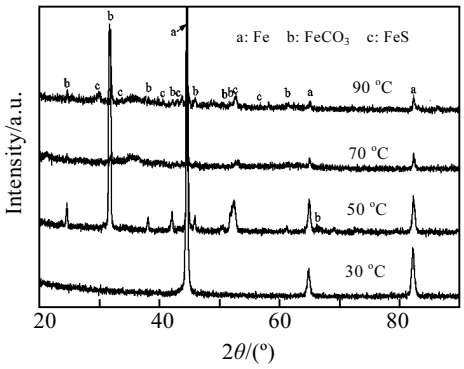

Fig.4 XRD patterns for the surface films formed on P110 tubing steel at different temperatures

Fig.5 presents the cross section morphologies of surface films formed on P110 tubing steel. It is evident that increasing temperature significantly enhances the formation of corrosion products, and makes a much thicker corrosion film. In Fig.5a, the corrosion film formed at 70 °C is the dark layer with a thickness of ~10 m. In Fig.5b, the corrosion film formed at 90 °C is the slightly grey layer with a thickness of ~ 20 m. The different contrast in the back scattered electron images for the corrosion films formed at two different temperatures may be related to the relative content of $FeCO_3$ and FeS. With temperature increasing, the relative content of FeS in the corrosion film increases, leading to a relatively obvious contrast in the back scattered electron images. EDS line scan result (Fig. 6) indicates that the corrosion film formed on P110 tubing steel at 90 °C is composed of iron, sulfur, carbon and oxygen, corresponding to the $FeCO_3$ and FeS as identified before.

After removal of corrosion films by chemical cleaning, surface morphologies of the corroded specimens are shown in Fig.7. Corrosion pits can be seen on the specimens corroded at 50, 70, and 90 °C. In addition, the size and quantity of corrosion pits increases with temperature.

On the basis of the above results, it can be speculated that increasing temperature can affect the corrosion behavior of P110 tubing steel in three aspects: enhancing the corrosion rate, promoting the formation of FeS and inducing pit corrosion.

2.2 Electrochemical behavior

Fig.8 illustrates the polarization curves of P110 tubing steel in the simulated environment at different temperatures. The obvious passivation area on the anodic polarization curve at 30 °C tends to disappear as temperature increases. This may be ascribed to the fast formation of corrosion products at higher temperatures which reduce the formation of passive film. It indicates that the corrosion film formed at 30 °C is more easily passivated than those formed at 50 and 70 °C. This means that the cathodic process of corrosion

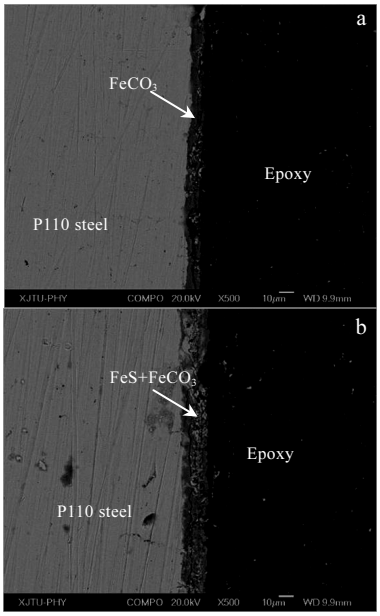

Fig.5 Cross section morphologies of surface films formed on P110 tubing steel at 70 °C (a) and 90 °C (b)

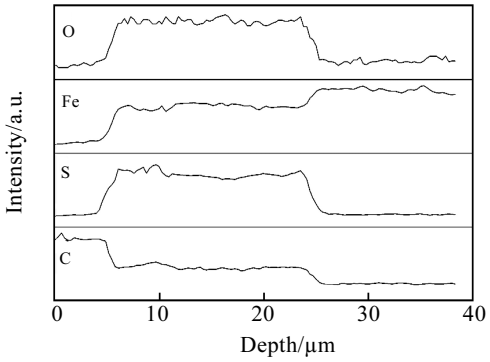

Fig.6 EDS line scan (in depth) result of the corrosion film formed on P110 tubing steel at 90 °C

reaction at 30 °C is controlled by concentration polarization instead of activated polarization. When the electrode potential is higher, the cathodic polarization current density is kept constant, and the limit current is independent of the electrode potential, so the corrosion reaction is controlled by the diffusion process. This is in accordance with the observations elsewhere[25].

Corrosion parameters calculated from polarization curves are summarized in Table 3. It can be seen that the cathodic Tafel slope is always greater than the anodic Tafel slope in the temperature range of 50~70 °C, indicating that the over potential of cathodic process is greater than that of anodic process so that the corrosion reaction is controlled by the cathodic process. With the increase of temperature, the corrosion current density increases obviously from 3.71 A/cm^2 to 148.7 A/cm^2, and the corrosion is accelerated. At 30

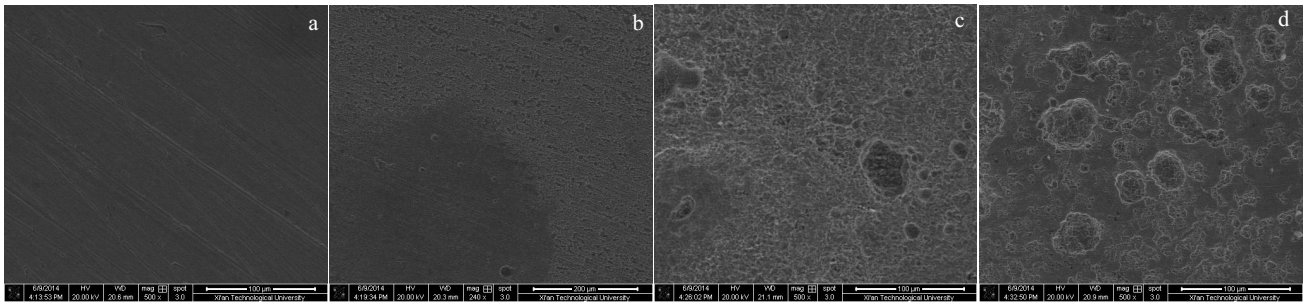

Fig.7 Surface morphologies of the corroded specimens at different temperatures after removal of corrosion films: (a) 30 °C, (b) 50 °C, (c) 70 °C, and (d) 90 °C

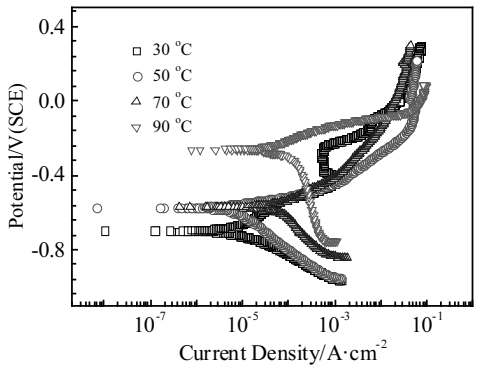

Fig.8 Polarization curves of P110 tubing steel at different temperatures

Table 3 Fitting parameters of polarization curves of P110 tubing steel in simulated solution at different temperatures

T/°C	b_a/ (mV/dec)	b_c/ (mV/dec)	I_{corr}/ μA·cm^{-2}	E_{corr}/ mV	R_p/ Ω·cm^2
30	91.9	68.3	3.71	–697.2	4585.7
50	52.9	189.4	5.98	–573.6	3002.5
70	87	235	10.9	–572.4	2529.4
90	106	192.3	148.7	–261.4	199.5

~ 70 °C, the increase of corrosion current density is slow, showing that the influence of temperature is slight. At 90 °C, the corrosion current density increases sharply, indicating the corrosion rate of P110 tubing steel is significantly enhanced. This is in accordance with the observation as mentioned above.

The impedance spectra of P110 tubing steel in the simulated environment at different temperatures are shown in Fig.9. It can be seen that all impedance spectra are composed of a capacitive arc located at the high frequency part and a Warburg impedance located at the low frequency part. There is significant difference on the radius of capacitance arc at the high frequency part. At 30 °C and 50 °C, similar AC impedance spectra containing double layer capacitance arc at high frequency and two time constants can be seen. However, the capacitive arc radius and reaction resistance R_t are relatively smaller at 50 °C, possibly because the increasing temperature enhances the activity of reactant, weakens the activation control, and accelerates the corrosion reaction. At 70 °C, the radius of capacitive arc is greater than that at 50 °C, which may be ascribed to the rather different microstructures of corrosion film. At 90 °C, the diffusion impedance is shown as a line with a large deviation from 45 °C, which may be caused by the dispersion effect due to the inhomogeneity of the electrode surface. There are two possible causes for the inhomogeneity: (i) pitting corrosion induced by elemental sulfur and Cl^-; (ii) accelerated localized corrosion induced by the local acidification between the iron sulfide and substrate.

3 Discussions

Based on the above results, it can be inferred that the increase of temperature can affect the corrosion of P110 tubing steel in the simulated environment from following aspects: enhancing the corrosion rate, promoting the formation of FeS and inducing pit corrosion.

For the uniform corrosion of P110 tubing steel in the simulated environment, competition between CO_2 corrosion and elemental sulfur corrosion determines the corrosion rate and corrosion products.

Concerning the CO_2 corrosion, it has been well recognized that the dissolved CO_2 gas in aqueous solution hydrates to form carbonic acid and results in corrosion of mild steels[26,27]. It is often assumed that hydrogen gas and bicarbonate ions are generated via the direct reduction of carbonic acid at the metal surface. However, more recently, it is considered that the dissociation of carbonic acid to hydrogen ions is the most important cathodic reaction in an acidic solution[15, 28-30]. In this perspective, the carbonic acid would act as a reservoir of hydrogen ions. As a result, the corrosion rate would be higher than strong acid solutions

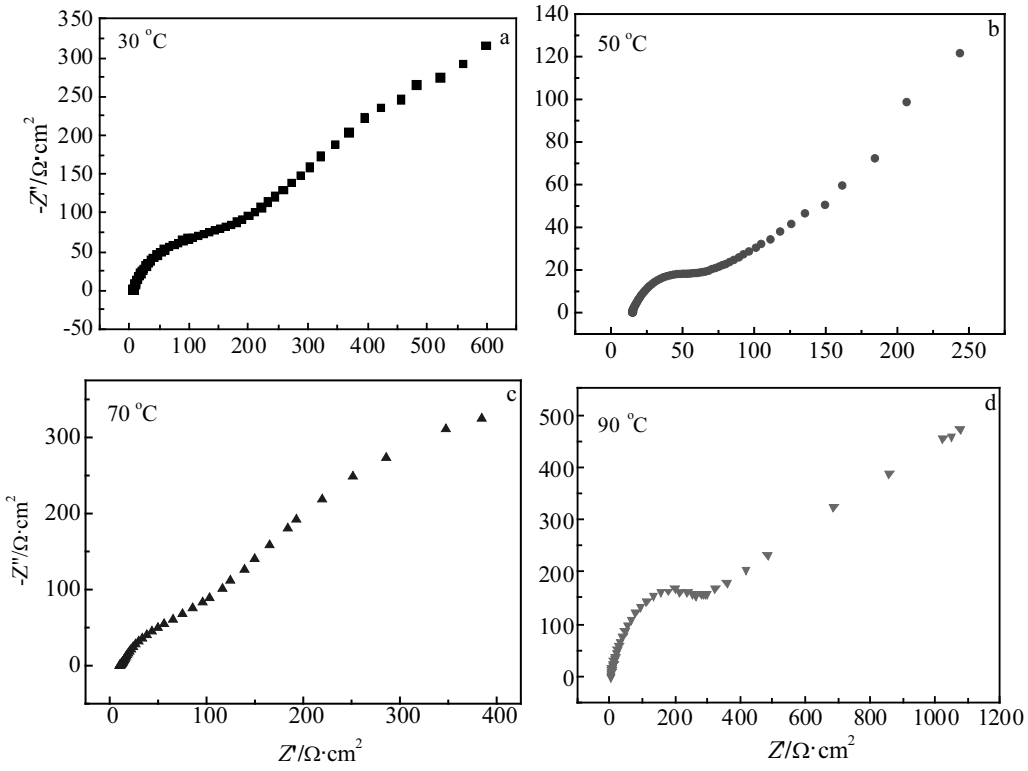

Fig.9 Impedance spectra results of P110 tubing steel at different temperatures: (a) 30 °C, (b) 50 °C, (c) 70 °C, and (d) 90 °C

under the same pH condition[31]. Solid $FeCO_3$ precipitates following Eq.(2):

$$Fe^{2+} + CO_3^{2-} = FeCO_3 \quad (2)$$

when the concentrations of relevant ions (i.e. Fe^{2+} and CO_3^{2-}) exceed their solubility limit. The precipitation of $FeCO_3$ would reduce the corrosion rate significantly. In addition, the precipitation rate is dependent on the $FeCO_3$ solubility limit. Sun et. al.[32] developed a unified expression for $FeCO_3$ solubility which is determined by temperature and ionic strength, as shown in Eq.(3):

$$\log K_{sp} = -59.3498 - 0.041377T_k - 2.1963/T_k + 24.5724\log(T_k) + 2.518I^{0.5} - 0.657I \quad (3)$$

where K_{sp} is the $FeCO_3$ solubility limit (mol^2/L^2) and I is the ionic strength (mol/L), and T_k is temperature.

In the present work, the ionic strength of the simulated solution is ~0.67 mol/L calculated from Eq.(4):

$$I = 1/2 \sum c_i z_i^2 = 1/2 (c_1 z_1^2 + c_2 z_2^2 + \cdots) \quad (4)$$

where c_i represents the concentrations of species in the solution (mol/L) and z_i represents the species charges. The calculated K_{sp} at studied temperatures are 4.89×10^{-10} (at 30 °C), 3.50×10^{-10} (at 50 °C), 2.28×10^{-10} (at 70 °C), and 1.37×10^{-10} (at 90 °C), indicating a decreasing trend with temperature increasing. It can be speculated that increasing temperature would promote the precipitation of iron carbonate as predicted by Sun et al [33]. However, increasing temperature almost reduces the corrosion rates of carbon steels in CO_2 containing aqueous environments[34-37]. On the one hand, increase in temperature would exacerbate corrosion by facilitating the following aspects: electrochemical reactions, molecular diffusion, and precipitation of iron carbonate. On the other hand, increasing temperature would reduce corrosion by retarding the following aspects: CO_2 solubility and solubility of iron carbonate. Among the possible aspects affected by increasing temperature, those causing the fast formation of protective iron carbonate scale are critical to the corrosion rate. At high temperature, the lower solubility and higher precipitation of iron carbonate results in the very dense and protective iron carbonate films and then reduces the corrosion rate[24].

Regarding the elemental sulfur corrosion, acidification by sulfur hydrolysis is often considered to be the main reason. Boden et al.[38] proposed sulfur hydrolysis controlled the elemental sulfur corrosion, as shown in Eq.(5):

$$S_8 + 8H_2O = 6H_2S + 2H_2SO_4 \quad (5)$$

Fang et al. [39] measured the pH value in the sulfur containing solution and found significant acidification of the solution at temperatures above 80 °C. They also reported

the sulfuric acid as a likely product of sulfur hydrolysis by ion chromatography analysis [38] and the concentration of sulfuric acid increased with temperature. From this perspective, the hydrolysis of elemental sulfur at 90 °C produces a large amount of H_2S and H_2SO_4, so that the concentrations of H^+, HS^-, and S^{2-} in the solution increase greatly. The reduction of H^+ and the dissolution of iron would be enhanced significantly. On the other hand, due to the stronger adsorption capacity of sulfur hydrolysis product like HS^- and S^{2-} than carbonic acid dissociation products like HCO_3^- and CO_3^{2-}, formation of iron sulfide is preferable[20].

Based on above discussion, the corrosion process of P110 tubing steel in the CO_2-saturated simulated oilfield formation water with element sulfur addition would be as follows. First, at low temperatures ($T \leq 50$ °C), CO_2 in the environment dominantly causes uniform corrosion and forms iron carbonate scale on the steel surface, while elemental sulfur causes little effect on the corrosion behavior. Second, in the moderate temperature range (50 °C $< T \leq$ 70 °C), corrosion is still controlled by CO_2 predominantly; however, elemental sulfur hydrolysis proceeds slightly and results in the formation of little amount of iron sulfide in the corrosion products. Third, as temperature increases above 70 °C, the corrosion-controlling reaction changes from dissociation of carbonic acid to sulfur hydrolysis, and leads to a corrosion scale primarily consisting of iron sulfide. Although the rising rate of corrosion rates along with temperatures decreases slightly after 70 °C, the corrosion rate at 90 °C is ~38% higher than that at 70 °C. This may be related to the weak scale contact as shown in Fig.3 where evident exfoliation and cracking can be seen.

4 Conclusions

The corrosion behavior of P110 tubing steel in CO_2-saturated simulated oilfield formation water with element sulfur addition was evaluated by immersion tests and electrochemical measurements. Increasing temperature accelerates the corrosion rate of P110 tubing steel, promotes the formation of iron sulfide, and causes serious pitting corrosion. Based on the results and discussion, following conclusions can be summarized.

1) At low temperatures ($T \leq 50$ °C), CO_2 in the environment dominantly causes uniform corrosion and forms iron carbonate scale on the steel surface, while elemental sulfur causes little effect on the corrosion behavior.

2) In the moderate temperature range (50 °C $< T \leq$ 70 °C), corrosion is still controlled by CO_2 predominantly; however, elemental sulfur hydrolysis proceeds slightly and results in the formation of little amount of iron sulfide in the corrosion products.

3) At temperature above 70 °C, the corrosion-controlling reaction changes from dissociation of carbonic acid to sulfur hydrolysis, and leads to a corrosion scale primarily consisting of iron sulfide.

References

1 Fu A Q, Feng Y R, Cai R *et al. Engineering Failure Analysis*[J], 2016, 66: 566

2 Zhang L, Wen Z, Li X *et al. NACE International Corrosion Conference & Expo*[C]. NACE, Houston, Texas: Paper No. 11121, 2011

3 Wang Chunguang, Wang Dongzhe, Liu Haiding *et al. Materials for Mechanical Engineerin*[J], 2017, 41(2): 85 (in Chinese)

4 Cai Xiaowen, Ge Lei, Yu Haobo *et al. Journal of Materials Science and Engineering*[J], 2010, 28(2): 226 (in Chinese)

5 Santos J P L, Lima Lobato A K C, Moraes C *et al. Journal of Petrolum Science and Engineering*[J], 2015, 135: 461

6 Liu Zhide, Lu Minxu, Gu Tan *et al. Corrosion and Protection* [J], 2012, 33(S2): 85 (in Chinese)

7 Liu W, Dou J, Lu S *et al. Appllied Surface Science*[J], 2016, 367: 438

8 Liu Zhiyong, Zhao Tianliang, Liu Ranke *et al. Journal of Central Sourth University*[J], 2016, 23: 757

9 Ochoa Nathalie, Vega Carlos, Pebere Nadine *et al. Materials Chemistry and Physics*[J], 2015, 156: 198

10 Li W, Pots B F M, Brown B *et al. Corrosion Science*[J], 2016, 110: 35

11 Xu L, Xiao H, Shang W *et al. Corrosion Science*[J], 2016, 109: 246

12 Liu QY, Mao L J, Zhou S W. *Corrosion Science*[J], 2014, 84: 165

13 Zhang J, Wang Z L, Wang Z M *et al. Corrosion Science*[J], 2012, 65: 397

14 Gao X, Brown B, Nesic S. *NACE International Corrosion Conference & Expo*[C]. NACE, San Antonio, Taxas, Paper No 3880, 2014

15 Tran T, Brown B, Nesic S. *NACE International Corrosion Conference & Expo*[C]. NACE, Houston, Texas, Paper No 5671, 2015

16 Addis K, Singer M, Nesic S. *Corrosion*[J], 2014, 70: 1175

17 Liu Q Y, Mao L J, Zhou S W. *Corrosion Science*[J], 2014, 84: 165

18 Eliyan F F, Alfantazi A. *Corrosion Science*[J], 2014, 85: 380

19 Sousa F V V, Viana P R P, Tribollet B *et al. Journal of the Electrochemical Society*[J], 2017, 164(6): C294

20 Fang H, Brown B, Young D *et al. NACE International Corrosion Conference & Expo*[C]. NACE, Houston, Texas: Paper No 11398, 2011

21 Jiang Xiu, Zhang Yanling, Qu Dingrong *et al. Corrosion Science and Protection Technology*[J], 2014, 26: 312 (in Chinese)

22 Fan Zhou, Li Hongchuan, Liu Jianyi *et al. Natural Gas*

Industry[J], 2013, 33: 102 (in Chinese)
23 Wei L, Zhang Y, Pang X *et al. Corrosion Reviews*[J], 2015, 33(3-4): 151
24 Hernandez J, Munoz A, Genesca J. *Afinidad*[J], 2012, 69: 251
25 Wei Huirong, Xiong Jinping, Zhao Jingmao *et al. Oilfield Chemistry*[J], 2011, 28: 342 (in Chinese)
26 Nesic S, Postlethwaite J, Olsen S. *Corrosion*[J], 1996, 52: 280
27 Kahyarian A, Singer M, Nesic S. *Journal of Natural Gas Science and Engineering*[J], 2016, 29: 530
28 Remita E, Tribollet B, Sutter E *et al. Corrosion Science*[J], 2008, 50: 1433
29 Amri J, Gulbrandsen E, Nogueira R P. *NACE International Corrosion Conference & Expo*[C]. NACE, Houston, Texas, Paper No 329, 2011
30 Tran T, Brown B, Nesic S *et al. Corrosion*[J], 2013, 70: 223
31 Nesic S. *Uhlig's Corrosion Handbook, 3rd ed*[M]. Hoboken, New Jersey: John Wiley & Sons, Inc, 2011: 229
32 Sun W, Nesic S, Woollam R C. *Corrosion Science*[J], 2009, 51: 1273
33 Sun W, Nesic S. *Corrosion*[J], 2008, 64: 334
34 Yin Z F, Feng Y R, Zhao W Z *et al*. *Surface and Interface Analysis*[J], 2009, 41: 517
35 Tanupabrungsun T, Young D, Brown B *et al. NACE International Corrosion Conference & Expo*[C]. NACE, Houston, Texas Paper No C2012-0001418, 2012
36 Lu Y, Jing H, Han Y *et al. Materials Chemistry and Physics* [J], 2016, 178: 160
37 Elgaddafi R, Naidu A, Ahmed R *et al. Journal of Natural Gas Science and Engineering*[J], 2015, 27: 1620
38 Boden P J, Maldonado-Zagal S B. *British Corrosion Journal* [J], 1982, 17: 116
39 Fang H, Young D, Nesic S. *NACE International Corrosion Conference & Expo*[C], 2008, Paper No 08637

P110 油管钢在含 S 元素和 CO_2 模拟油田地层水饱溶液中的腐蚀行为研究

苗 健[1,2]，袁军涛[2]，韩 燕[2]，徐秀清[2]，李 磊[2]，王 珂[2]

(1. 西安交通大学，陕西 西安 710049)

(2. 中国石油天然气集团公司管材研究所 石油管材及装备材料服役行为与结构安全国家重点实验室，陕西 西安 710077)

摘 要：随着对油气资源需求量的高速增长，高含硫油气藏不断被开发，由于元素硫、CO_2、以及地层水等多腐蚀因素的耦合作用，带来了高的油套管腐蚀风险。通过浸泡试验和电化学试验研究了 P110 油管钢在含元素硫和 CO_2 的模拟油田地层水中的腐蚀行为。结果表明，随着温度升高，促进了硫化亚铁的形成，P110 油管钢的腐蚀速率增大，并发生了严重的局部腐蚀。然而，温度在不同的范围内的影响是不同的，这主要是由于不同的腐蚀控制因素，如低温下受二氧化碳控制，而高温下主要受元素硫控制。最后，基于这些结果讨论了元素硫和二氧化碳的耦合效应。

关键词：P110 油管钢；元素硫；腐蚀；地层水；CO_2 腐蚀

作者简介：苗 健，男，1980 年生，博士生，西安交通大学材料科学与工程学院，陕西 西安 710049，E-mail: miaojian001@cnpc.com.cn